Biosensors and Bioelectronics 244 (2024) 115808

Contents lists available at ScienceDirect

Biosensors and Bioelectronics

journal homepage: www.elsevier.com/locate/bios

Exploration of aminopeptidase N as new biomarker for early diagnosis of thyroid cancer

Lanlan Xu [a], Mo Ma [a,c], Jingkang Li [a], Dianfeng Dai [a], Dejiang Gao [a], Pinyi Ma [a,**], Qiong Wu [b,***], Daqian Song [a,*]

[a] College of Chemistry, Jilin Province Research Center for Engineering and Technology of Spectral Analytical Instruments, Jilin University, Qianjin Street 2699, Changchun, 130012, China
[b] Key Laboratory of Pathobiology, Ministry of Education, Nanomedicine and Translational Research Center, The Third Bethune Hospital of Jilin University, Sendai Street 126, Changchun, 130033, China
[c] School of Pharmacy, Jilin University, Qianjin Street 2699, Changchun, 130012, China

ARTICLE INFO

Keywords:
Aminopeptidase N
Thyroid cancer
Fluorescence probe
Imaging in cells
Imaging *in vivo*

ABSTRACT

False-positive diagnosis and overdiagnosis are ongoing issues in clinical diagnosis of thyroid cancer. Identifying new disease markers is crucial for early diagnosis and improved treatment. Aminopeptidase N (APN) is a promising biomarker for cancer diagnosis due to its critical roles in tumor invasion, metastasis, angiogenesis, and other processes. However, its potential as biomarker for thyroid cancer diagnosis needs further investigation. This study developed an ultra-sensitive near-infrared fluorescence probe, LAN-apn, to investigate the expression level of APN in thyroid cancer and evaluate its potential as biomarker of thyroid cancer. LAN-apn could accurately and sensitively determine APN through fluorescence method (DL = 0.069 ng/mL) and colorimetric method (DL = 4.5 ng/mL). In addition, LAN-apn allowed for successful fluorescence imaging of APN in thyroid cancer cells and thyroid cancer tumors both *in vivo* and *in vitro*, and confirmed that APN was significantly upregulated in thyroid cancer. Therefore, APN may become a new biomarker for thyroid cancer diagnosis, and LAN-apn could be used as a new imaging tool for the study of APN-thyroid cancer relationship and the early diagnosis of thyroid cancer.

1. Introduction

Thyroid cancer is a highly diverse solid malignancy (Kebebew, 2018) and the endocrine malignancy (Gallardo et al., 2020; Silva, 2021) most commonly found in women of reproductive age (Crump et al., 2016; Toro-Wills et al., 2022). Although the prognosis of thyroid cancer is generally favorable compared to other cancers, it can still have a significant psychological impact on patients (Lopez Gavilanez et al., 2020). Overdiagnosis of clinically insignificant lesions is a growing concern (Boukheris and Bachir Bouiadjra, 2022; McDow et al., 2020) due to the increased use of high-resolution cervical ultrasonography and fine needle aspiration (Cho et al., 2017; Morris et al., 2016). Currently, thyroglobulin is used as a disease marker to track thyroid cancer (Haugen et al., 2016; Zahra et al., 2021), but the presence of thyroglobulin antibodies can generate false positive signals (Lee et al., 2020; Rosario et al., 2021), which emphasizes the need for new disease markers for early diagnosis of thyroid cancer.

Aminopeptidase N (APN/CD13, EC 3.4.11.2) is a dimeric membrane protein that belongs to the zinc metallopeptidase family (Chen et al., 2012). It is widely distributed in mammals and plays a role in various physiological and pathological processes, including signal transduction, neuropeptide degradation, immune responses, and antigen processing (Bauvois and Dauzonne, 2006; Mina-Osorio, 2008). Due to its importance in tumor invasion, metastasis, angiogenesis, and other processes (Hata et al., 2016; Mawrin et al., 2010; Wickstrom et al., 2011), APN has been identified as a promising biomarker for cancer (Huang et al., 2020; Li et al., 2020). Several APN- mediated fluorescent probes have been developed for imaging liver cancer (Ma et al., 2023), breast cancer (Liu et al., 2021b), cervical cancer (Yang et al., 2023), bladder cancer (Huang et al., 2020), and lung cancer (Liu et al., 2022). However, the potential

* Corresponding author.
** Corresponding author.
*** Corresponding author.
E-mail addresses: mapinyi@jlu.edu.cn (P. Ma), qiong_wu@jlu.edu.cn (Q. Wu), songdq@jlu.edu.cn (D. Song).

https://doi.org/10.1016/j.bios.2023.115808
Received 15 August 2023; Received in revised form 15 October 2023; Accepted 30 October 2023
Available online 2 November 2023

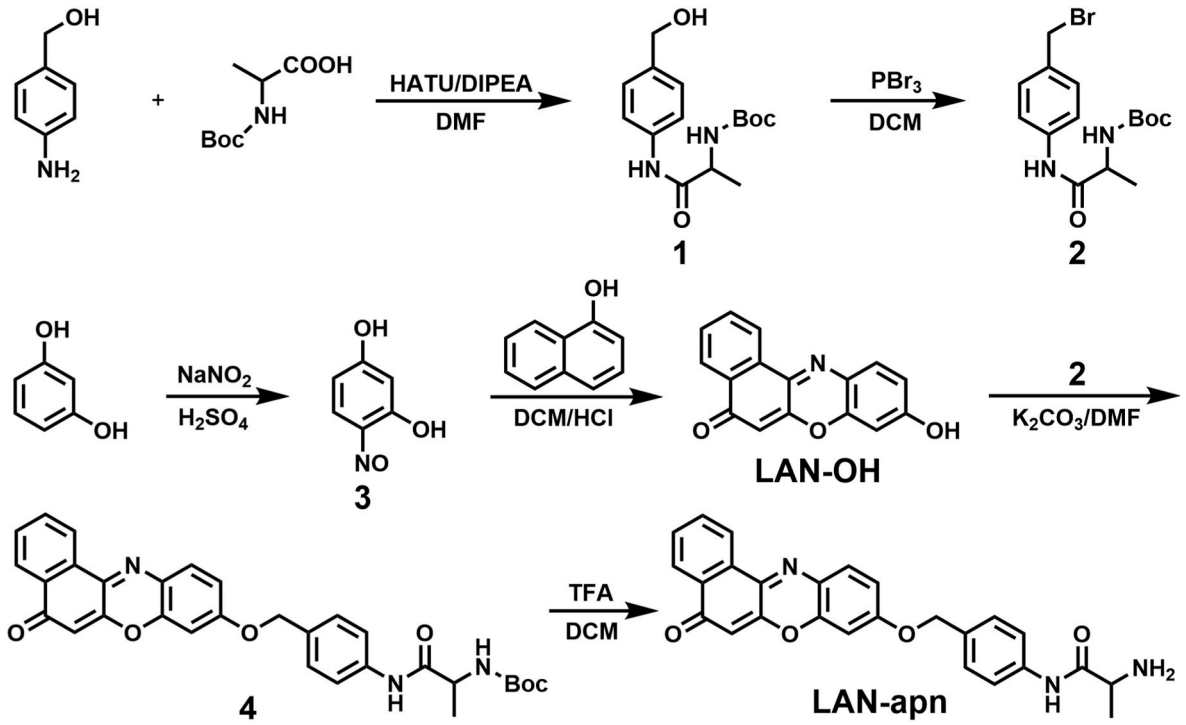

Scheme 1. Synthetic route of probe LAN-apn.

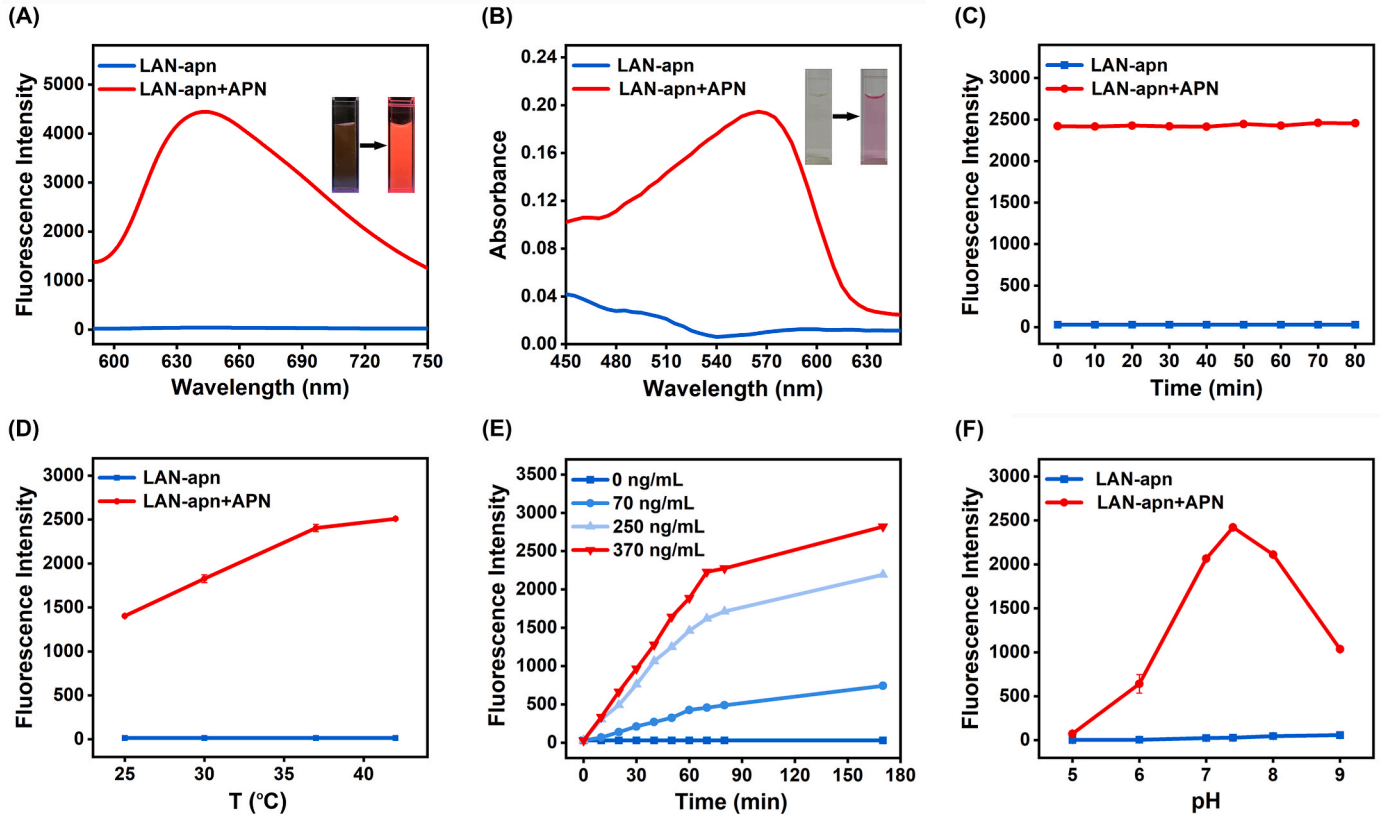

Fig. 1. (A)/(B) Fluorescence/absorption spectra of 10 μM LAN-apn and reaction system (10 μM LAN-apn with 1000 ng/mL APN). (C) Photostability of 10 μM LAN-apn and reaction system (10 μM LAN-apn with 400 ng/mL APN). (D) Temperature-dependent fluorescence intensity of 10 μM LAN-apn and reaction system (10 μM LAN-apn with 400 ng/mL APN). (E) Time-dependent fluorescence intensity of 10 μM of LAN-apn in the presence or absence of APN at various concentrations. (F) pH-dependent fluorescence intensity of 10 μM LAN-apn and reaction system (10 μM LAN-apn with 400 ng/mL APN).

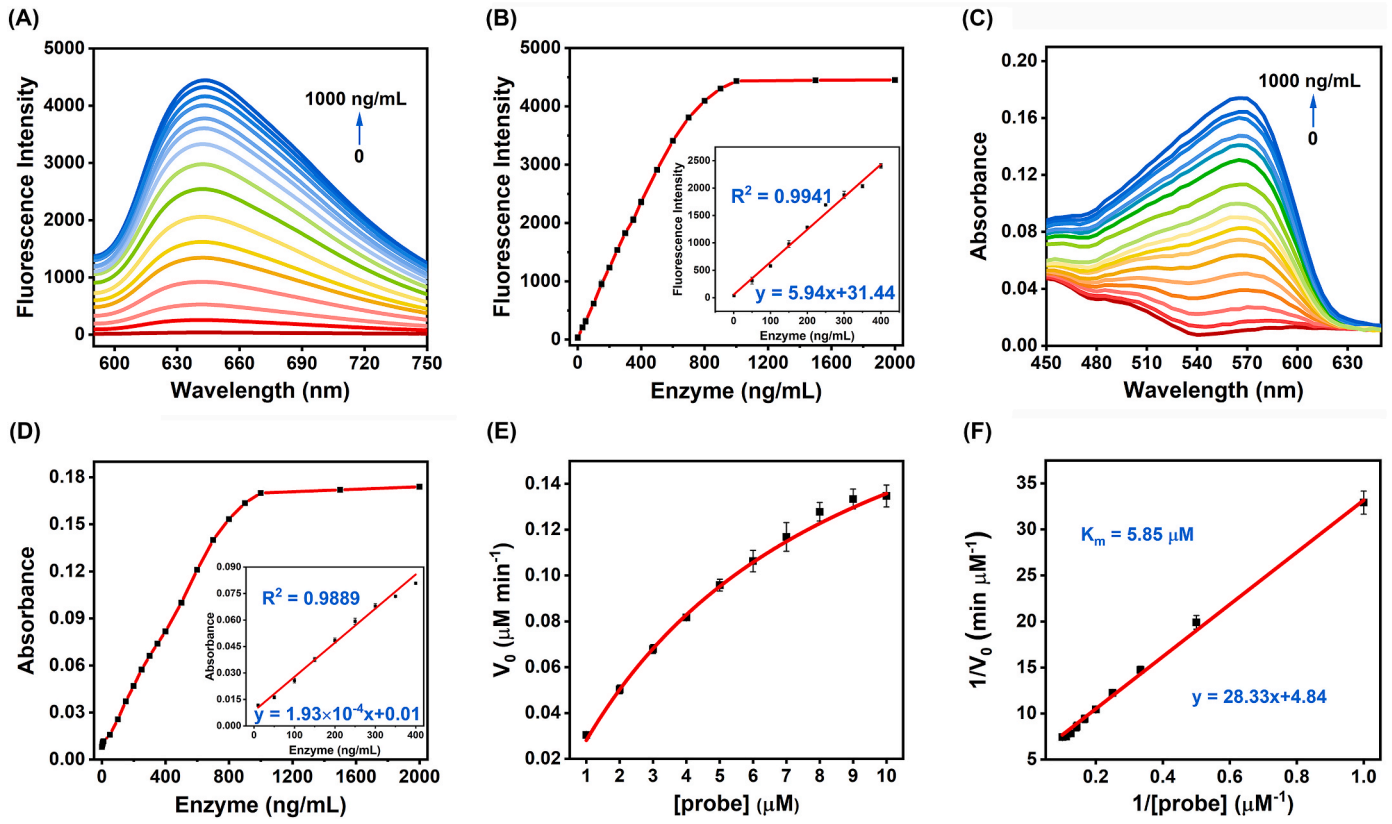

Fig. 2. (A) Fluorescence spectra of 10 μM LAN-apn in the presence of APN at various concentrations. (B) Linear relationship between fluorescence intensity at 642 nm of reaction system and APN concentrations (1–400 ng/mL). (C) Absorption spectra of 10 μM LAN-apn in the presence of APN at various concentrations. (D) Linear relationship between absorbance at 575 nm of reaction system and APN concentrations (10–400 ng/mL). (E) Michaelis-Menten plot for enzymatic reaction between APN (270 ng/mL) and LAN-apn at various concentrations (1, 2, 3, 4, 5, 6, 7, 8, 9, and 10 μM). (F) Lineweaver-Bulk plot of the enzymatic reaction.

of APN as biomarker for thyroid cancer diagnosis remains to be explored. Given the increasing incidence of thyroid cancer and the need for more accurate and reliable diagnostic markers, investigating the potential of APN as a diagnostic marker for thyroid cancer can be significantly valuable.

In this study, an ultra-sensitive near-infrared fluorescence probe LAN-apn was developed to evaluate the potential of APN as biomarker for tracking thyroid cancer. LAN-apn was characterized for its high stability, good water solubility, high sensitivity, and selectivity, and used for imaging of APN in living system, verified the upgradation of APN level in thyroid cancer. Thus, APN may serve as a biological target for tracking thyroid cancer and could potentially lead to the development of improved diagnostic tools for thyroid cancer.

2. Experimental procedure

2.1. Organic synthesis

The synthetic route of LAN-apn is shown in Scheme 1. **Compound 1**, **2**, **3** and **LAN-OH** were synthesized according to previously reported strategies (Feng et al., 2021; Xu et al., 2020, 2023).

Synthesis of compound 4. Compound LAN-OH (0.263 g, 1 mmol), compound 2 (0.356 g, 1 mmol), and K_2CO_3 (0.138 g, 1 mmol) were successively added into 10 mL of N,N-Dimethylformamide (DMF) and stirred for 3 h at room temperature. Next, saturated salt water was poured into the reaction flask, and the generated precipitate was further purified by silica gel column chromatography (CH_2Cl_2:CH_3OH = 30:1) to obtain compound 4 as yellow solid (73% yield).

Synthesis of probe LAN-apn. Compound 4 (0.24 g, 0.446 mmol) was dissolved in 5 mL of CH_2Cl_2. Next, 1 mL of trifluoroacetic (TFA) acid was added dropwise into the reaction flask and stirred for 1 h at room temperature. Then, saturated salt water was poured into the reaction flask. After stratification, the organic layer was collected and then further purified by silica gel column chromatography (CH_2Cl_2:CH_3OH = 20:1) to obtain probe LAN-apn as yellow solid (80% yield). ^{1}H NMR (500 MHz, DMSO-d_6) δ 10.85 (s, 1H), 8.56 (d, J = 7.6 Hz, 1H), 8.11 (d, J = 7.8 Hz, 1H), 7.96 (s, 1H), 7.85 (t, J = 6.9 Hz, 1H), 7.78 (dd, J = 15.0, 8.1 Hz, 2H), 7.71 (d, J = 8.5 Hz, 2H), 7.48 (d, J = 8.5 Hz, 2H), 7.14 (d, J = 2.6 Hz, 1H), 7.07 (dd, J = 8.8, 2.6 Hz, 1H), 6.36 (s, 1H), 5.20 (s, 2H), 4.05 (d, J = 7.0 Hz, 1H), 1.46 (d, J = 7.0 Hz, 4H) (Fig. S1). ^{13}C NMR (126 MHz, DMSO-d_6) δ 182.51, 168.85, 162.33, 161.28, 151.28, 145.13, 143.63, 138.35, 132.15, 131.48, 131.39, 131.07, 130.64, 128.81, 127.02, 125.16, 123.99, 119.40, 113.76, 105.91, 101.26, 69.94, 49.11, 35.80, 30.79, 17.52 (Fig. S2). MS (m/z) for $C_{26}H_{22}N_3O_4^+$ $[M+H]^+$: calculated, 440.1610; found: 440.1618 (Fig. S3).

2.2. Detection of APN in solution

Firstly, probe LAN-apn was dissolved in Dimethyl sulfoxide (DMSO) to prepare 1 mM stock solution. 1 mL sample containing 10 μM LAN-apn, a certain concentration of analyte, and PBS (10 mM, pH 7.4) was subjected to analysis by a fluorescence spectrometer and a UV–vis spectrophotometer. The reaction system was incubated at 37 °C in PBS buffer solution (10 mM, pH 7.4) containing 1% (v/v) DMSO for 70 min (unless otherwise stated) before detection.

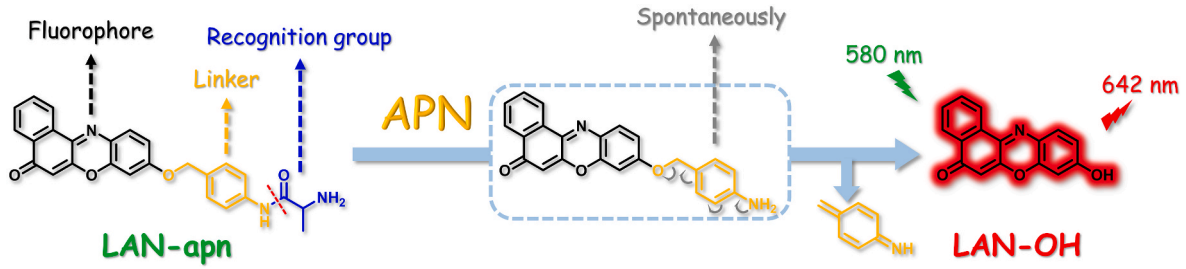

Fig. 3. Proposed detection mechanism of LAN-apn towards APN.

3. Results and discussion

3.1. Characterization of LAN-apn

Fluorescence and absorption spectra of LAN-apn were analyzed. The fluorescence spectrum (Fig. 1A) demonstrated that the addition of APN significantly increased the emission peak intensity of LAN-apn at 642 nm (λ_{ex} = 580 nm) and caused the solution color to change from yellow to bright red under ultraviolet light at 365 nm. The absorption spectrum (Fig. 1B) showed that the addition of APN significantly enhanced the absorption peak intensity of LAN-apn at 575 nm, accompanied by a visible solution color change from light yellow to red. These findings indicate that LAN-apn could effectively detect APN using fluorescence and colorimetric methods.

Next, the photostability of LAN-apn was investigated, and the results (Fig. 1C) showed that the fluorescence intensity of both LAN-apn and the reaction system did not change significantly under the irradiation of 580-nm light for 80 min, indicating the good photostability. The effect of temperature on LAN-apn (Fig. 1D) showed that the fluorescence intensity of LAN-apn remained almost unchanged at the temperature range of 25–42 °C, suggesting that LAN-apn has good thermal stability. By contrast, the fluorescence intensity of the reaction system gradually increased with increasing temperature, indicating that increasing temperature to a certain range can accelerate the enzymatic reaction. The change in fluorescence intensity of the reaction system with time was investigated. As can be observed in Fig. 1E, the fluorescence intensity of the reaction system increased rapidly before 70 min and then slowly. The effect of pH on LAN-apn is shown in Fig. 1F. The fluorescence intensity of LAN-apn remained stable, while that of the reaction system gradually increased with pH until reaching the maximum value at pH 7.4 and then gradually decreased. It can be inferred that APN has a lower activity in acidic and alkaline environments but a higher activity at pH 7.4. Based on the above results and considering the physiological conditions, all subsequent experiments were conducted in PBS (10 mM, pH 7.4) at 37 °C for 70 min before test.

3.2. Analytical performance of LAN-apn

Under the optimal conditions, the analytical performance of LAN-apn was evaluated by fluorescence and colorimetric methods. The fluorescence spectra (Fig. 2A and B) demonstrated that the fluorescence intensity at 642 nm of the reaction system gradually increased with increasing APN concentration (λ_{ex} = 580 nm). Additionally, a satisfactory linear relationship (r = 0.9971) was observed between the fluorescence intensity and APN concentrations at a range of 1–400 ng/mL (DL = 0.069 ng/mL). LAN-apn was found to be analytically superior to other reported fluorescence probes in terms of fluorescence enhancement, excitation/emission wavelengths and DL, as shown in Table S1. The colorimetric method (Fig. 2C and D) showed that the absorbance at 575 nm of the reaction system increased with increasing APN concentration, and a good linear relationship (r = 0.9944) was observed between the absorbance and APN concentrations at a range of 10–400 ng/mL (DL = 4.5 ng/mL). In summary, LAN-apn could quantitatively detect APN via fluorescence and colorimetric methods.

The enzyme kinetic between LAN-apn and APN was further investigated. According to the Michaelis-Menten plot (Fig. 2E) and Lineweaver-Burk plot (Fig. 2F), the Michaelis constant (K_m) 5.85 μM, which is far below that of alanyl-p-nitroaniline (K_m = 0.74 mM). The value of 1 /K_m is generally used to approximate the enzyme affinity to the substrate, that is, the greater the value of 1 /K_m, the greater the affinity of the enzyme to the substrate, and the easier the enzymatic reaction to carry out. Combined with the low detection limit (LOD = 0.069 ng/mL) and low quantitation limit (LOQ = 0.23 ng/mL) of the probe for APN, we fully confirmed that LAN-apn has good affinity and high sensitivity for APN.

3.3. Selectivity of LAN-apn

High selectivity is a crucial property for probe that allows for accurate detection of an analyte without interference from other substances in complex systems. In order to assess the selectivity of LAN-apn to APN, effects from a series of common potential interferents on LAN-apn were examined. As depicted in Fig. S4, the presence of interfering substances at high concentrations had no discernible impacts on LAN-apn. In contrast, the presence of APN significantly impacted LAN-apn, which is likely attributed to the presence of alanine, an APN-specific recognition group (Li et al., 2019; Liu et al., 2021a; Ma et al., 2023), in LAN-apn. In addition, the results from enzyme kinetic (Fig. 2E and F) indicated that LAN-apn has good affinity and high sensitivity to APN. The above results are indicative of the high selectivity of LAN-apn to APN.

3.4. Sensing mechanism

Mass spectrometric analysis, HPLC analysis and inhibitor experiment were conducted to explore the sensing mechanism of LAN-apn towards APN. The results of mass spectrometric analysis showed that LAN-apn exhibited a mass peak at m/z 440.1618 (Fig. S3), and LAN-OH at m/z 264.0667 (Fig. S5), while the reaction system exhibited a mass peak at m/z 264.0657 (Fig. S6), which basically matched with that of LAN-OH. HPLC analysis (Fig. S7) revealed the characteristic peaks of LAN-apn and LAN-OH at 1.60 min and 2.52 min, respectively, while the reaction system exhibited the characteristic peaks at both 1.60 min and 2.52 min, corresponding to the peaks of LAN-apn and LAN-OH, respectively. The results of inhibitor experiment (Fig. S8) confirmed that bestatin had little impact on the fluorescence intensity of both LAN-apn and LAN-OH, but significantly inhibited the fluorescence intensity of the reaction system. Based on above results, the sensing mechanism of LAN-apn (Φ_F < 0.001, τ = 1.52 ns) towards APN can be that APN specifically recognizes and digests alanine in LAN-apn, causing the p-aminobenzyl alcohol linker to detach ultimately leading to the release of LAN-OH (Φ_F = 0.47), allowing APN to be detected by LAN-apn (Fig. 3).

3.5. Molecular docking and theoretical calculations

Molecular docking simulation (Figs. S9A and S9B) showed that LAN-apn forms five hydrogen bonds with four amino acids (Pro432, Gln693,

Table 1
Recovery rates of APN spiked into human urine (n = 3).

Sample	APN added (ng/mL)	Found by LAN-apn[a] (ng/mL)	Recovery (%)	Found by ELISA kit[a] (ng/mL)	Recovery (%)
Blank	0.00	12.98±0.33	–	14.91±0.01	–
1	20.00	33.26±1.52	101.4	34.74±0.01	99.1
2	40.00	52.80±0.92	99.6	55.91±0.03	102.5
3	60.00	69.03±2.12	93.4	74.19±0.01	98.8

[a] Mean ± standard deviation.

Tyr689, and Ser697) in APN with a binding energy of −10.4 kcal/mol, suggesting that LAN-apn has strong binding affinity to APN. The molecular orbitals of LAN-apn and LAN-OH, calculated using TDDFT, are presented in Fig. S9C. Both the HOMO and LUMO of LAN-apn are predominantly localized within the entire fluorophore. In contrast, LAN-OH shows no significant redistribution of electronic density on its HOMO and LUMO. Despite this absence of electronic density redistribution, TDDFT calculations revealed a typical ICT occurring at 625.7 nm (S_1 to S_0, f = 1.1193), which leads to strong fluorescence from LAN-apn upon its reaction with APN. Furthermore, the energy gap for LAN-OH is lower (2.58 eV) compared to that of LAN-apn (2.99 eV), logically accounting for the observed redshift in the absorption wavelengths of LAN-apn, both in the absence and presence of APN. These findings support the sensing mechanism proposed in Fig. 3.

3.6. Recovery rate of APN in urine

Early studies have demonstrated that APN levels in urine are significantly increased due to kidney damage and pathological changes (Cheng et al., 2020; Dominguez et al., 2023). As a result, APN can serve as a sensitive indicator for evaluating renal injury, which is valuable for diagnosing kidney diseases. Clinical analytical community had studied the amount of APN in serum and urine for healthy adults, but there are no reported standardized absolute concentration range values of APN for a healthy control currently available (Kumaravel et al., 2022). To evaluate the ability of LAN-apn to accurately detect APN in urine, LAN-apn was used to measure the recovery rates of APN spiked into human urine. The results presented in Table 1 showed that the recovery rates of 20.00, 40.00, and 60.00 ng/mL APN in urine samples ranged from 93.4% to 101.4%. To verify the accuracy of probe LAN-apn, the human urine samples were also tested by commercial ELISA kit for comparison. The results showed that the error between the ELISA kit and the probe method was within 7.4%, indicating that probe LAN-apn can accurately detect APN in human urine.

3.7. Visualization of APN in cells

Before being applied to cell imaging, LAN-apn was first evaluated for its cytotoxicity by CCK-8 assay. The results (Fig. S10) showed that cells incubated with LAN-apn at concentrations as high as 50 μM had viability of over 90%, which is indicative of the low cytotoxicity of LAN-apn.

Changes of intracellular fluorescence intensity with time were investigated. As shown in Fig. S11, the intracellular fluorescence

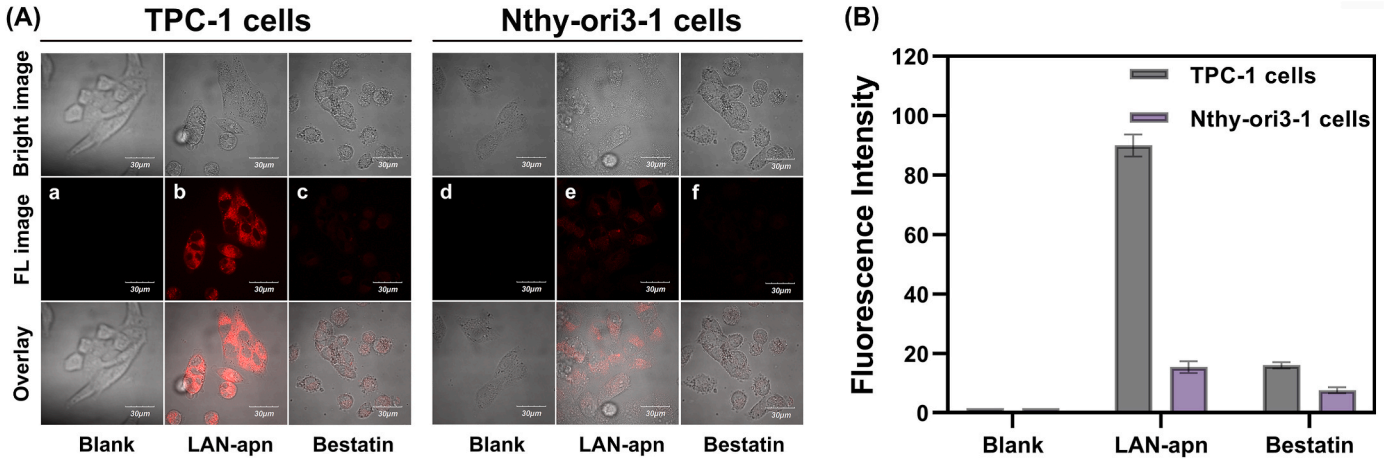

Fig. 4. (A) Fluorescence images of endogenous APN in living cells. (B) Mean fluorescence intensity values of cells in (A).

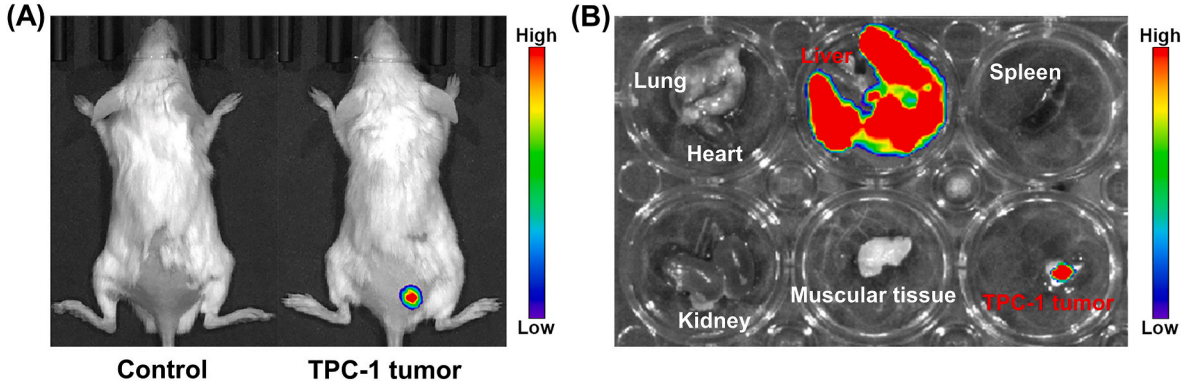

Fig. 5. (A) Fluorescence images of control mouse and TPC-1 tumor-bearing mouse injected with LAN-apn (200 μM, 50 μL). (B) *In vitro* imaging of living tissues incubated with 200 μM LAN-apn.

intensity gradually increased over time until reaching its maximum value at about 60 min and remained unchanged for at least 120 min. Thus, a 60-min incubation time was used in subsequent imaging experiments of LAN-apn.

Next, LAN-apn was applied to fluorescence imaging to assess the expression of endogenous APN in TPC-1 cells (thyroid cancer cells) and Nthy-ori3-1 cells (normal thyroid cells). The results showed (Fig. 4) weak fluorescence signals in Nthy-ori3-1 cells (e) but strong fluorescence signals in TPC-1 cells (b). Moreover, the addition of bestatin (an inhibitor of APN) significantly inhibited the intracellular fluorescence signals, especially for TPC-1 cells, which indicates that APN level is significantly upregulated in thyroid cancer cells, and LAN-apn can effectively visualize endogenous APN in cells.

3.8. Visualization of APN in vivo

Encouraged by the satisfactory cell imaging results, we further investigated the expression of APN levels *in vivo*. As shown in Fig. 5A, the mouse in the control group almost did not exhibit fluorescence signals, while the TPC-1 tumor-bearing mouse exhibited significant fluorescence signal at the tumor site, which was consistent with the cell imaging results. These results suggested that APN level was up-regulated in thyroid tumors, and LAN-apn can be used to visualize early-stage thyroid tumors.

3.9. Imaging of living tissues in vitro

The APN levels in various organs were investigated. As shown in Fig. 5B, heart, spleen, lung, kidney, and muscle tissues did not exhibit observable fluorescent signals. In contrast, strong fluorescent signals were observed in the liver and TPC-1 tumor, which was an indication that the APN level was up-regulated in TPC-1 tumor. These findings demonstrate that LAN-apn is a powerful tool for *in vitro* imaging and evaluation of APN levels.

4. Conclusions

In this study, we designed and synthesized an ultra-sensitive near-infrared fluorescent probe, LAN-apn, to investigate the expression level of APN in thyroid cancer and evaluate its potential as biomarker of thyroid cancer. Probe LAN-apn with high stability, good solubility, good selectivity and high sensitivity, could accurately and sensitively determine APN through fluorescence method and colorimetric method. In bioimaging, LAN-apn could specifically “light up” APN in cells and tumors both *in vivo* and *in vitro*, confirmed the overexpression of APN in thyroid cancer. Thus, it is apparent that APN has the potential to become a new clinical marker for the diagnosis of thyroid cancer, and LAN-apn can become a promising new imaging tool for the early diagnosis of thyroid cancer. However, we acknowledge several important considerations for real-world clinical application. Firstly, our sample size was limited, necessitating further validation across diverse populations and disease stages. Additionally, the long-term stability of LAN-apn and its cost-effectiveness compared to existing diagnostic methods require evaluation. Lastly, clinical validation with a larger cohort is essential to comprehensively assess its diagnostic utility. In the future work, we will pay more attention to the structure optimization of probe LAN-apn to realize Point-of-Care testing and multiplexed assay, and to validate the clinical application of probe LAN-apn in a larger, more diverse patient population. These efforts collectively aim to bring LAN-apn closer to clinical implementation, offering an effective, reliable, and accessible diagnostic tool for thyroid cancer.

CRediT authorship contribution statement

Lanlan Xu: Conceptualization, Investigation, Data curation, Validation, and, Writing – original draft, preparation. **Mo Ma:** Data curation, Investigation, Investigation, for biological experiments. **Jingkang Li:** Data curation, Investigation. **Dianfeng Dai:** Data curation, Investigation. **Dejiang Gao:** Formal analysis, and, Software. **Pinyi Ma:** Conceptualization, Project administration, Data curation, Writing – review & editing, and, Software. **Qiong Wu:** Investigation, Resources, Writing – review & editing, and, Software. **Daqian Song:** Project administration, Funding acquisition, Resources, Supervision.

Declaration of competing interest

The authors declare that they have no known competing financial interests or personal relationships that could have appeared to influence the work reported in this paper.

Data availability

Data will be made available on request.

Acknowledgement

This work was supported by the National Natural Science Foundation of China (22004046 and 22074052) and the Science and Technology Developing Foundation of Jilin Province of China (Nos. 20230101033JC, 20220505015ZP and YDZJ202302CXJD031).

Appendix A. Supplementary data

Supplementary data to this article can be found online at https://doi.org/10.1016/j.bios.2023.115808.

References

Bauvois, B., Dauzonne, D., 2006. Med. Res. Rev. 26 (1), 88–130.
Boukheris, H., Bachir Bouiadjra, N., 2022. Eur. J. Cancer Prev. 31 (3), 301–308.
Chen, L., Lin, Y.L., Peng, G., Li, F., 2012. Proc. Natl. Acad. Sci. USA 109 (44), 17966–17971.
Cheng, P., Miao, Q., Huang, J., Li, J., Pu, K., 2020. Anal. Chem. 92 (8), 6166–6172.
Cho, Y.J., Kim, D.Y., Park, E.C., Han, K.T., 2017. BMC Cancer 17 (1), 114.
Crump, C., Sundquist, J., Sieh, W., Winkleby, M.A., Sundquist, K., 2016. Int. J. Cancer 138 (5), 1085–1093.
Dominguez, M., Meyer, K., Sancenon, F., Blandez, J.F., Serrano, M., Martinez-Manez, R., 2023. Chem. Commun. 59 (17), 2481–2484.
Feng, L., Tian, Z., Zhang, M., He, X., Tian, X., Yu, Z., Ma, X., Wang, C., 2021. Chin. Chem. Lett. 32 (10), 3053–3056.
Gallardo, E., Medina, J., Sanchez, J.C., Viudez, A., Grande, E., Porras, I., Ramon, Y.C.T., Trigo, J., Iglesias, L., Capdevila, J., 2020. Clin. Transl. Oncol. 22 (2), 223–235.
Hata, R., Nonaka, H., Takakusagi, Y., Ichikawa, K., Sando, S., 2016. Angew. Chem. Int. Ed. 55 (5), 1765–1768.
Haugen, B.R., Alexander, E.K., Bible, K.C., Doherty, G.M., Mandel, S.J., Nikiforov, Y.E., Pacini, F., Randolph, G.W., Sawka, A.M., Schlumberger, M., Schuff, K.G., Sherman, S.I., Sosa, J.A., Steward, D.L., Tuttle, R.M., Wartofsky, L., 2016. Thyroid 26 (1), 1–133.
Huang, J., Jiang, Y., Li, J., He, S., Huang, J., Pu, K., 2020. Angew. Chem. Int. Ed. 59 (11), 4415–4420.
Kebebew, E., 2018. J. Natl. Cancer Inst. 110 (4), 327–328.
Kumaravel, S., Luo, G.-R., Huang, S.-T., Lin, H.-Y., Lin, C.-M., Lee, Y.-C., 2022. Biosens. Bioelectron. 203, 114049.
Lee, Z.J.O., Eslick, G.D., Edirimanne, S., 2020. Thyroid 30 (11), 1601–1612.
Li, H., Li, Y., Yao, Q., Fan, J., Sun, W., Long, S., Shao, K., Du, J., Wang, J., Peng, X., 2019. Chem. Sci. 10 (6), 1619–1625.
Li, H., Yao, Q., Sun, W., Shao, K., Lu, Y., Chung, J., Kim, D., Fan, J., Long, S., Du, J., Li, Y., Wang, J., Yoon, J., Peng, X., 2020. J. Am. Chem. Soc. 142 (13), 6381–6389.
Liu, S.-Y., Wang, H., Zou, X., Nie, G., 2022. Sensor. Actuat. B-Chem. 363, 131828.
Liu, Y., Xu, C., Liu, H.W., Teng, L., Huan, S., Yuan, L., Zhang, X.B., 2021. Anal. Chem. 93 (16), 6463–6471.
Lopez Gavilanez, E., Bautista Litardo, N., Navarro Chavez, M., Hernandez Bonilla, M., Segale Bajana, A., 2020. BMC Cancer 20 (1), 637.
Ma, M., Dai, D., Ma, P., Wu, Q., Gao, D., Song, D., 2023. Sensor. Actuat. B-Chem. 379, 133228.
Mawrin, C., Wolke, C., Haase, D., Kruger, S., Firsching, R., Keilhoff, G., Paulus, W., Gutmann, D.H., Lal, A., Lendeckel, U., 2010. Brain Pathol. 20 (1), 200–210.
McDow, A.D., Zahnd, W.E., Angelos, P., Mellinger, J.D., Ganai, S., 2020. J. Rural Health 36 (3), 326–333.
Mina-Osorio, P., 2008. Trends Mol. Med. 14 (8), 361–371.
Morris, L.G., Tuttle, R.M., Davies, L., 2016. JAMA Otolaryngol. 142 (7), 709–711.

Rosario, P.W., Cortes, M.C.S., Franco Mourao, G., 2021. Endocr. Relat. Cancer 28 (4), R111–R119.
Silva, S.N., 2021. Genes 12, 126.
Toro-Wills, M.F., Imitola-Madero, A., Alvarez-Londono, A., Hernandez-Blanquisett, A., Martinez-Avila, M.C., 2022. Womens Health 18, 17455057221136392.
Wickstrom, M., Larsson, R., Nygren, P., Gullbo, J., 2011. Cancer Sci. 102 (3), 501–508.
Xu, L., Chu, H., Gao, D., Wu, Q., Sun, Y., Wang, Z., Ma, P., Song, D., 2023. Anal. Chem. 95 (5), 2949–2957.
Xu, L., Wu, M., Zhao, L., Han, H., Zhang, S., Ma, P., Sun, Y., Wang, X., Song, D., 2020. Talanta 215, 120892.
Yang, J., Shen, C., Zhu, T., Qian, Q., Diao, X., Huang, W., Yasen, W., Su, Y., Zhu, X., Shi, L., 2023. Biomater. Sci. 11, 2809.
Zahra, H.O., Omran, G.A., Gewely, A.G., Eldehn, A.F., Abdo, W., Elmahallawy, E.K., Okda, T.M., 2021. Diagnostics 11, 2080.